# Exploring MERRA-2 global meteorological and aerosol reanalyses for improved SST retrieval

Xin Xi[1,2], Alexander Ignatov[1], Xinjia Zhou[1,2]

[1]NOAA STAR, NCWCP, College Park, MD 20740, USA

[2]CSU CIRA, Fort Collins, CO 80523, USA

Corresponding author:

Xin Xi (xin.xi30@gmail.com)

5830 University Research Court

College Park, MD 20740

Keywords:

Sea surface temperature; dust; aerosol correction; MERRA; VIIRS

Abstract

This study explores the use of Modern-Era Retrospective analysis for Research and Applications version 2 (MERRA-2) global meteorological and aerosol reanalysis for improving the simulation of satellite sensor infrared brightness temperatures (BTs), and the retrieval of sea surface temperature (SST) in the NOAA Advanced Clear Sky Processor for Ocean (ACSPO) system, with a particular focus on ACSPO long-term reprocessing efforts. Using MERRA-2 upper-air pressure, temperature, and humidity profiles, rather than the currently used NCEP Global Forecast System (GFS) real-time data, as input into the Community Radiative Transfer Model (CRTM), reduces the global clear-sky observation-minus-model (O–M) BT biases in the infrared bands centered at 3.7, 8.6, 11, and 12 μm of the Visible Infrared Imaging Radiometer Suite onboard Suomi-NPP. The improvements are largely due to more accurate water vapor (total amount and/or vertical distribution) at low latitudes in MERRA-2, which brings the modeled BTs closer to observations. Additional stand-alone simulations, performed using RTTOV model and MERRA-2 aerosol profiles, further reduce the ACSPO global O–M BT biases and the dependence of O–M BT biases on the dust aerosol optical depth. The potential skill of MERRA-2 aerosol reanalysis for reducing dust-caused regional biases in the ACSPO global regression SST product is also demonstrated. Preliminary results suggest that MERRA-2 is a viable alternative to NCEP GFS for ACSPO reprocessing efforts.

## 1. Introduction

Sea surface temperature (SST) is routinely retrieved from brightness temperatures (BTs) measured by a number of passive infrared (IR) spaceborne sensors in the atmospheric window regions. SST retrieval typically uses multi-channel or non-linear SST (MC/NLSST) regression algorithms to account for the atmospheric attenuation by water vapor. Customarily, split-window bands centered at 11 and 12 μm are used, often in conjunction with the more transparent shortwave band centered at 3.7 μm (e.g., Prabhakara et al., 1974; McMillin, 1975; McMillin and Crosby, 1984). Other window bands (e.g., centered at 8.6 μm) may also be included, when available.

At NOAA, the Advanced Clear-Sky Processor for Ocean (ACSPO) enterprise system is employed to produce SSTs from several polar-orbiting and geostationary sensors. As part of its processing, ACSPO calculates the expected top-of-atmosphere (TOA) clear-sky sensor BTs using the Community Radiative Transfer Model (CRTM), in conjunction with first-guess SST (currently, Canadian Meteorological Center (CMC) daily L4 analysis; Brasnett and Surcel-Colan, 2016) and atmospheric profiles of pressure, temperature, water vapor, and ozone (currently, from the National Centers for Environmental Prediction Global Forecast System, NCEP GFS) (e.g., Liang et al., 2009). The observation-minus-model (O–M) BT biases are used to monitor the SST bands of different sensors for stability and cross-platform consistency, validate the CRTM and its inputs, improve ACSPO clear-sky mask, and explore physical SST retrieval. Currently, no aerosol absorption or scattering is included in the CRTM employed in ACSPO, which may be one of several factors contributing to the persistent cold O–M biases of several tenths of a Kelvin, depending on sensors and bands, as observed in the NOAA Monitoring of IR Clear-sky Radiances over Ocean for SST (MICROS) system (Liang and Ignatov, 2011).

Several sensitivity studies have been conducted in the past, towards more accurate modeling of sensor BTs in ACSPO. Liang et al. (2009) tuned the CRTM and optimized in-pixel CRTM calculations for satellite sensors with resolutions from 1-4 km, using low-resolution first-guess CMC SST (0.2º) and GFS profiles (1º). Saha et al. (2012) compared several SST L4 analyses as input into CRTM and selected the CMC product, which best captured the spatial variability in satellite derived SSTs and was most stable in time. Liang et al. (2017) examined the sensitivity of modeled BTs to the use of European Center for Medium-Range Weather Forecasts (ECMWF) profiles, instead of NCEP GFS, and found that ECMWF data reduced the global O–M BT biases. Both ECMWF and GFS are real-time data, whereas for the ACSPO reanalysis (e.g., Ignatov et al., 2016), long-term uniform data sets are needed, which preferably include aerosol first-guess fields to explore including aerosol in BT simulations, and aerosol corrections to SST.

Following the El Chichon (1982) and Mt. Pinatubo (1991) eruptions, additions to the MC/NLSST formulations have been explored to correct for the effect of sulfate aerosols, whose absorption spectra differ from those of water vapor (Griggs, 1985; Reynolds, 1993; Merchant et al., 1999). In the presence of IR-absorbing aerosols, the deviations of satellite BTs from SST are approximately linearly related to two factors: the slant path IR aerosol optical depth (AOD), and the temperature contrast between the aerosol layer and sea surface (Griggs, 1985). While the slant path AOD at visible wavelengths may predict, to some degree, the effect of volcanic aerosols on the BTs and derived SST, due to the relatively well known and nearly fixed vertical distribution in the stratosphere, it may be less effective for predicting the BT and SST biases due to tropospheric aerosols, because of the highly variable optical properties and vertical distributions (May et al., 1992; Nalli and Stowe, 2002). In particular, wind-blown dust from the deserts of Africa, Arabian Peninsula, and Asia is often responsible for persistent seasonal SST biases over the North Atlantic, Arabian Sea, and West Pacific (Diaz et al., 2001). Through radiative transfer simulations, Merchant et al. (2006) derived a Saharan dust index from the BT differences in the four IR bands used for SST retrieval. The SDI has shown some skill to account for the effects of dust amount and vertical profile on the SST bias, thus improving the SST retrieval over the North Atlantic. Note that the SDI can only be derived from nighttime data, due to solar contamination in the 3.7 µm band (Good et al., 2012; Le Borgne et al., 2013), and its application with daytime data requires additional efforts.

Previous simulations of dust effects on BTs and SSTs were limited by the use of idealized configurations of dust concentrations and vertical placement. Thanks to recent advances in aerosol observations and modeling, several weather prediction centers have developed global aerosol reanalyses, in conjunction with conventional meteorological fields, such as the Modern-Era Retrospective analysis for Research and Applications version 2 (MERRA-2) (Buchard et al., 2017; Gelaro et al., 2017). These newly available data have the potential for improving satellite BT simulations for a globally representative range of meteorological and aerosol conditions.

This study explores the utility of MERRA-2 global meteorological reanalysis, instead of NCEP GFS, for improving the simulation of sensor BTs under aerosol-free conditions, for the use in ACSPO reprocessing efforts. The effect of MERRA-2 meteorological profiles on ACSPO global O–M BT biases is presented based on global nighttime data from the Visible and Infrared Imaging Radiometer Suite (VIIRS) onboard the Suomi-NPP satellite. In addition, we preliminarily evaluate the skill of MERRA-2 aerosol reanalysis to bring modeled BTs closer to observations. Dust aerosol attenuations of VIIRS BTs based on stand-alone RTTOV model simulations are used to correct the sensor BTs, and subsequently, the ACSPO global regression SST. This strategy differs from past studies in that the aerosol correction based on radiative transfer simulations is applied directly to sensor BTs, thereby minimizing possible changes in the SST equations and potentially enabling aerosol correction for both daytime and nighttime SSTs.

## 2. Approach

MERRA-2 consists of a collection of land, atmosphere, and aerosol products for the modern satellite era generated by the NASA Goddard Earth Observing System version 5 data assimilation system (GEOS-5), which assimilates meteorological observations and bias-corrected AOD observations from satellites and ground stations (Gelaro et al., 2017). The MERRA-2 meteorological fields are available at 42 pressure levels from 1000 to 0.1 hPa every 3 hours at 0.5°×0.625° resolution. The MERRA-2 aerosol fields are provided at 72 model layers, and converted to the same pressure levels as the meteorological fields. Compared to MERRA-2, the NCEP GFS meteorological data are available at 26 pressure levels from 1000 to 10 hPa every 6 hours at 1°×1° resolution. The pressure, temperature and humidity profiles from MERRA-2 and GFS are used as input into two separate simulations using ACSPO (v2.50) to calculate the VIIRS BTs in the 3.7, 8.6, 11, and 12 μm bands. Both simulations use the CMC L4 as the first-guess SST. Results shown in this study are based on simulations using two weeks' global nighttime data between 18–31 January 2018.

Currently, the CRTM in ACSPO is not capable of incorporating external information of aerosol optical properties and vertical profiles in BT simulations. Hence, the RTTOV model (v12.1) is used to evaluate the potential of MERRA-2 aerosol reanalysis for improving sensor BT simulations and SST retrieval under dusty conditions. RTTOV has been used in previous studies to simulate the BT responses to aerosol loadings for a number of sensors (Merchant et al., 2006; Good et al., 2012; Le Borgne et al., 2013). Here two RTTOV experiments are conducted for the VIIRS clear-sky pixels under aerosol-free and dust-affected conditions, respectively. During the study period of 18–31 January 2018, large amounts of dust aerosol are blown off the deserts of West Africa to the Atlantic Ocean, and off Arabian Peninsula to the Red Sea, Persian Gulf, and Arabian Sea. The difference between the two RTTOV simulations is calculated as the dust-induced BT changes, which are used for aerosol correction to sensor BTs. To simulate the dust effect on sensor BTs, RTTOV requires profiles of dust absorption and scattering coefficients and backscatter parameters. These profiles are generated in three steps: 1) the MERRA-2 dust mixing ratios at five size bins are multiplied by the extinction coefficients at 0.55 μm (which are provided by the GEOS-5 model) and added to generate the profile of visible (0.55 μm) AOD; 2) The visible AOD is converted to IR AOD at 10 μm, as $AOD_{10\mu m} = 0.4 \times AOD_{0.55\mu m}$. The ratio of IR to visible AOD ranged from 0.2 to 0.6, and was found to decrease with the distance away from the source area, as the coarse mode particles are preferentially removed during atmospheric transport (Pierangelo et al., 2004). A ratio of 0.4 is used in this study for the mid-range transport to Cape Verde islands, where dust causes strong attenuation of sensor BTs. 3) The extinction AOD at 10 μm is further separated to the absorption and scattering AODs at VIIRS IR bands, based on Mie-computed dust absorption and scattering properties (Xi and Sokolik, 2012). The assumption of dust particles as spheres in Mie calculations has negligible effects in the IR wavelengths (Yang et al., 2007). The Mie calculations use refractive index and size distribution from the Optical Properties of Aerosols and Clouds (OPAC) database (Hess et al., 1998). The aerosol backscatter parameter is then calculated from the Mie scattering phase function.

## 3. Results

While implementing CRTM in ACSPO, Liang et al. (2009) made various improvements to minimize the global O–M BT biases, which are measured by mean/median biases and conventional/robust standard deviations (SD/RSD). Conventional statistics are useful for evaluating the overall performance of ACSPO products, but may be sensitive to outliers in satellite data (due to e.g., residual cloud or sensor malfunction). In contrast, the robust statistics are less affected by outliers, and may be better suited to evaluate the performance of the forward model or retrieval method (Merchant et al., 1999; Liang and Ignatov, 2011). If the O–M BT biases have near Gaussian distributions (see Fig. 1), the conventional and robust statistics are close to each other. In this study, only the robust statistics will be discussed. The results will be shown based on the entire simulation period, unless noted otherwise.

3.1. Effects of MERRA-2 vs. GFS on O–M BT biases in aerosol-free conditions

Table 1 shows that using GFS profiles in ACSPO CRTM yields global O–M median biases of -0.145, -0.714, -0.575 and -0.728 K in the VIIRS bands centered at 3.7, 8.6, 11 and 12 μm, respectively. Possible causes for the cold O–M biases in all bands are either increased "M" (due to e.g., insufficient amount of water vapor and/or its inaccurate placement in the atmosphere, missing aerosols in GFS, or the use of foundation CMC L4, rather than the cooler skin SST, as input to the forward model), or decreased "O" (due to e.g., residual cloud in VIIRS observations) (Liang and Ignatov, 2011). The fact that the magnitude of the O–M bias is closer to zero in the most transparent 3.7 μm band and much larger in the less transparent longwave bands, suggests a possible "dry bias" in the GFS atmospheric profiles (or its not fully accurate vertical distribution, e.g., placing it lower in the atmosphere, closer to the warm sea surface).

Replacing GFS with MERRA-2 as input to ACSPO reduces the O–M biases and brings them closer to zero, in all SST bands. As shown in Table 1, the bias reduction is smallest at 3.7 μm (-0.031K). The improvement becomes progressively larger in the more absorbing bands at 8.6, 11, and 12 μm (-0.088, -0.111, and -0.129 K, respectively). The RSDs are also reduced (by -0.043, -0.124, -0.141, and -0.190 K respectively, in root-mean-square sense). Figure 2 further shows that the improvements in the O–M median biases and RSDs are consistent in all bands and for all days during the study period, after replacing GFS with MERRA-2 data.

To better understand the likely underlying causes of the O–M bias improvements, Figure 3a shows a highly linear relationship between the changes in the O–M biases (at the 3.7 μm band) and the difference in total precipitable water vapor (TPWV) between MERRA-2 and GFS. Note that for clarity, the O–M biases are binned by the water vapor difference. As expected, smaller column water vapor amounts in MERRA-2 result in a warmer bias, and larger water vapor amounts in a colder bias. Interestingly, the fit line in Fig. 3a does not go through the origin, suggesting that different vertical distributions of water vapor in MERRA-2 and GFS may also contribute to the simulated BT differences. Fig. 3b shows that the reduction in O–M biases is most prominent in the tropical region near the equator, where IR absorption by water vapor is strongest and the water vapor profile more critically affects the simulated BTs. This is consistent with the larger amount of TPWV in MERRA-2 at low- and mid-latitudes, as shown in Fig. 3c. Figure 3d further reveals that the TPWV difference is larger at the Western Hemisphere. However, the TPWV difference between MERRA-2 and GFS near the equator is not as strong as at mid-latitudes (e.g., 30$^{o}$S), which implies that at the equator, the difference in water vapor vertical distribution may also contribute to the peak in the simulated BT difference using MERRA-2 vs. GFS fields. Therefore, the improvements in the O–M bias statistics are likely due to the fact that MERRA-2 captures the global distribution of water vapor, both geographical and vertical, better than NCEP GFS. Such differences are probably better seen and captured in the absorption bands, but our analyses suggest that they are large enough, to cause statistically significant improvements even in the window bands employed for SST retrieval.

3.2. Effect of using RTTOV vs. CRTM on O–M BT biases in aerosol-free conditions

In ACSPO, CRTM simulations are performed over the GFS or MERRA-2 grids, and the simulated atmospheric radiances and transmittances are then bilinearly interpolated to VIIRS pixels. In contrast, the RTTOV simulations are performed directly on the sensor pixel level, which are performed here in a stand-alone mode (i.e., outside ACSPO framework). Table 1 shows that in the RTTOV simulations using MERRA-2 data, the global O–M biases under aerosol-free conditions are significantly reduced, and become much closer to zero, especially in the two longwave bands, to -0.087 K at 11 μm, and -0.096 K at 12 μm. The bias also decreases at 8.6 μm, but less dramatically, to -0.391 K. The inconsistency between the 8.6 and 11-12 μm bands has been noted and reported to the RTTOV developers’ team. However, as of the time of this writing, the possible causes of this inconsistency remain unclear. In the most transparent 3.7 μm band, the O–M bias even turns slightly positive, leaving no room for the remaining unaccounted physical factors discussed above (all of which are expected to result in negative O–M bias). Interestingly, the RSDs are consistently larger in RTTOV simulations, possibly due to increased noises in pixel-level simulations. Recall that the objective of RTTOV experiments here was to simulate the dust effects on VIIRS BTs for the use in testing the aerosol correction on SST retrieval. Comparison of the relative performance of CRTM and RTTOV is not straightforward with the current experiments, due to the implementation differences.

### 3.3. Effect of dust aerosols on the O–M BT biases

To simulate the effect of dust on sensor BTs, the MERRA-2 aerosol profiles are first interpolated onto the VIIRS clear-sky pixels. Figure 4a shows a global map of MERRA-2 total column dust AOD (0.55 μm) on January 23, 2018. Massive dust outflow can be seen from the deserts of West Africa and the Middle East to the North Atlantic and Arabian Sea, respectively. A relatively weak dust plume is also seen over the Pacific Ocean, which may be transported from the

Taklimakan and Gobi Deserts of East Asia. Although Asian dust is associated with lower AODs, the plume is lifted to higher altitudes (i.e., above 6 km) compared to African dust, as seen from the map of vertical height where dust AOD reaches maximum, $H_m$ (Fig. 4b).

Figure 4a and 4b also show that the low dust AODs (<0.02) are associated with highly variable $H_m$, ranging from close to the surface to the upper troposphere (>8 km). The density plot in Figure 4c reveals that these low AOD values cover the majority (>80%) of ocean regions. In contrast, the large AOD pixels, mostly located at the North Atlantic, fall within much tighter vertical heights below 4 km. Given that no aerosol height information is currently being assimilated in MERRA-2, the dust vertical profile may be uncertain, especially for the low AODs, which could be model noises. Therefore, the dust-affected RTTOV simulation is performed only for the pixels with a column AOD larger than 0.02 (0.55 μm), in order to reduce computational cost and minimize the influence of the data noises from MERRA-2.

The dust-induced BT changes in VIIRS IR bands are calculated as the differences between the dust-affected and aerosol-free RTTOV experiments. An example of the BT change in the 3.7 μm band is shown in Fig. 4d. The global average BT reduction due to dust is -0.07 K in this band. However, the BT reductions are not uniform in space, reaching -0.9 K over the North Atlantic and some parts of the Arabian Sea, due to the attenuation by strong dust load. In comparison, the BT changes are smaller over the Pacific, where Asian dust is greatly reduced after long range transport from inland sources (although it's lifted to higher altitudes and therefore potentially may cause more cooling in the BTs). There are also small BT reductions over the Black and Caspian Seas, which may be affected by dust transport from the deserts of Central Asia (Xi and Sokolik, 2015; Xi and Sokolik, 2016).

Figure 5 shows the O–M biases (calculated with CRTM and MERRA-2) as a function of dust AOD, in the original VIIRS O–M biases, and after correcting for the dust aerosol effect (calculated as the difference between two RTTOV runs, with and without dust). After aerosol correction, the dependence is greatly reduced (i.e., smaller slopes) in all bands, suggesting a statistically significant skill in the MERRA-2 aerosol reanalysis to correct for dust-induced effects on the sensor BTs. The improvement in dependency is however not complete, with all bands under-corrected. This could possibly be remedied by tuning the scaling factor of MERRA-2 visible AOD to IR AODs (a value of 0.4 is used in this study) in order to maximize the dust correction. The aerosol correction is also not uniform across the different bands, with the 11 μm band having the largest residual aerosol dependency. One possible cause might be the inaccurate spectral optical properties from the Mie calculations, which uses globally invariant dust refractive index and particle size distribution. More work is needed to better understand the cause of the incomplete and non-uniform aerosol correction in the top-of-atmosphere BTs.

### 3.4. Effect of aerosol correction on SST

Two SST products are currently generated in ACSPO: one using global regression (GR; Petrenko et al., 2014) and the other using piecewise regression (PWR; Petrenko et al., 2016) algorithms, respectively. The ACSPO GR SST is calculated using a single set of regression coefficients, trained on a global dataset of matchups, while the PWR derives different regression coefficients in several segments of the SST retrieval domain, which is defined by the SST equation regressors (Petrenko et al., 2016). The GR SST is known to be subject to significant regional and seasonal biases (Merchant et al., 2009), whereas the PWR SST was designed to empirically reduce all such regional and local biases, regardless of their physical causes (e.g., due to residual cloud, globally non-uniform distributions of water vapor and temperature profiles, angular dependencies in SST algorithms, etc.), and thus minimize the need for bias corrections in their assimilation into L4 analyses such as CMC. Our visual analyses in the NOAA SST Quality Monitor system (SQUAM; www.star.nesdis.noaa.gov/sod/sst/squam/; Dash et al., 2010) suggest that the PWR SST indeed significantly reduces regional biases, including over aerosol-affected areas, associated with Saharan, East Asia, and Saudi Arabian dust outbreaks. In this study, we estimate the skill of MERRA-2 aerosol reanalysis to reduce aerosol-induced biases in the GR SST, and compare it with the current skill provided by the empirical PWR SST.

Aerosol-corrected GR SST is re-computed from aerosol-corrected VIIRS BTs, using the same ACSPO GR equation and current operational regression coefficients. (Ideally, the regression coefficients should have been recalculated for “aerosol-free” BTs, to minimize the global satellite minus in situ biases). Therefore, some biases in the aerosol-corrected GR SST may be expected, but the objective is to compare the AOD dependencies in the aerosol-corrected vs. current non-corrected ACSPO GR SSTs, and the empirically-corrected PWR SST. The remaining global biases can be easily removed, if needed, by retraining the GR regression coefficients against the aerosol-corrected BTs.

Figure 6 (top panel) shows that the biases of all three SST products follow near-Gaussian distributions. The ACSPO GR SST has a median bias of -0.008 K and RSD of 0.242 K, compared to the bias of 0.074 K and RSD of 0.240 K for the aerosol-corrected GR SST. Note that non-zero biases in both GR SSTs are expected, due to the use of the operational ACSPO coefficients, not specifically optimized for the simulation period. Likewise, a slight degradation of the bias in the aerosol-corrected SST is also possible, because the regression is not retrained on aerosol-free BTs.

In contrast, the RSD in aerosol-corrected GR SST improve by -0.03 K, in root-mean-square sense. As shown in Fig. 7, the RSD of aerosol-corrected SST may deteriorate on certain days (such as the less dusty period of 30-31 January 2018), but over the two-week period, is reduced compared to the non-corrected SST. This result suggests some potential skill of the MERRA-2 aerosol reanalysis to correct the sensor BTs and SSTs. Considering the fact that all current aerosol analyses, including MERRA-2, are based on assimilation of AOD at visible wavelengths, and a lack of any direct assimilation of aerosol vertical distribution information which strongly affects the IR BTs and SSTs, we consider this a strong evidence of the utility of MERRA-2 aerosol reanalysis to predict the dust effects in the SST IR bands.

It is also interesting to compare the aerosol-corrected GR SST with the PWR SST, which has a bias of 0.036 K and RSD of 0.204 K, respectively. As expected, the RSD of PWR SST is significantly smaller than for both GR SSTs, prior to aerosol correction and after it, because the PWR attempts to reduce all biases in the SST product, including those caused by aerosols.

Another informative and relevant comparison of the skill of the physical aerosol-corrected versus empirical PWR SSTs, is the dependencies of the corresponding global mean biases on dust AOD, as shown in Fig. 6b. Although the PWR significantly reduces both magnitudes of the median biases and their dependencies on dust AOD, the aerosol-corrected GR SST provides the least dependency for both first and second moments of the distributions shown in Fig. 6b and 7. This suggests that applying the PWR regression, on the top of the aerosol-corrected GR SST, may further improve the accuracy of ACSPO SST products.

## 4. Conclusions

To facilitate the NOAA ACSPO SST reprocessing from a number of sensors, we explored the MERRA-2 meteorological and aerosol reanalyses for improving the monitoring of global O–M

BT biases and SST retrieval at four IR bands (centered at 3.7, 8.6, 11 and 12 μm, respectively) of SNPP VIIRS. Based on two weeks' global nighttime data (18-31 January 2018), we showed that the global O–M BT median biases are reduced, in all SST bands, likely due to more accurate water vapor (i.e., total amount and/or vertical placement) in MERRA-2, compared to the NCEP GFS real-time data currently used in ACSPO. The global RSDs for the O–M biases are also reduced, in all VIIRS SST bands.

Furthermore, accounting for the unwanted dust signal in sensor BTs using stand-alone RTTOV simulations, further reduces the global O–M BT median biases, RSDs, and dependencies on dust AOD. Using aerosol-corrected VIIRS BTs in the ACSPO global regression equation leads to reduced RSD in the aerosol-corrected SST, compared to the non-corrected global regression SST. More importantly, the aerosol correction greatly reduces the dependence of SST bias on the dust AOD, and does it even more effectively than the current ACSPO piecewise regression SST. Our findings suggest that MERRA-2 meteorological fields are a viable alternative to NCEP GFS real-time data for ACSPO reprocessing. Also, the MERRA-2 aerosol reanalysis demonstrates some potential skill for reducing dust-related BT and SST biases, but this requires more work and analyses, before it can be directly explored and fully implemented in the ACSPO system.

Acknowledgements

We thank M. Bosilovich, R. A. Lucchesi and J. V. Ardizzone for assistance with MERRA-2, and J. Hocking for help with RTTOV. MERRA-2 is obtained online from https://goldsmr5.sci.gsfc.nasa.gov/data/MERRA2/. RTTOV source code is obtained from EUMETSAT NWP SAF (https://www.nwpsaf.eu/site/software/rttov/). This manuscript benefits from discussions with X. Liang and B. Petrenko. We also thank two anonymous reviewers for their comments and suggestions. The views, opinions, and findings contained in this paper are

those of the authors and should not be construed as an official NOAA or US Government position, policy, or decision. The authors declare no conflicts of interest.

References

Brasnett, B., & Surcel-Colan, D. (2016). Assimilating retrievals of sea surface temperature from VIIRS and AMSR2**.** Journal of Atmospheric and Oceanic Technology, 33, 361-375. https://doi.org/10.1175/JTECH-D-15-0093.1

Buchard, V., Randles, C.A., da Silva, A.M., Darmenov, A., Colarco, P.R., Govindaraju, R., Ferrare, R., Hair, J., Beyersdorf, A.J., Ziemba, L.D., & Yu, H. (2017). The MERRA-2 Aerosol Reanalysis, 1980 Onward. Part II: Evaluation and Case Studies. Journal of Climate, **30**, 6851–6872. https://doi.org/10.1175/JCLI-D-16-0613.1

Dash, P., A. Ignatov, Y. Kihai, and J. Sapper (2010), The SST Quality Monitor (SQUAM), Journal of Atmospheric and Oceanic Technology, 27(11), 1899-1917. https://doi.org/10.1175/2010JTECHO756.1

Di Biagio, C., Formenti, P., Balkanski, Y., Caponi, L., Cazaunau, M., Pangui, E., Journet, E., Nowak, S., Caquineau, S., Andreae, M. O., Kandler, K., Saeed, T., Piketh, S., Seibert, D., Williams, E., & Doussin, J.-F. (2017). Global scale variability of the mineral dust long-wave refractive index: a new dataset of in situ measurements for climate modeling and remote sensing. Atmospheric Chemistry and Physics, 17, 1901-1929. https://doi.org/10.5194/acp-17-1901-2017

Diaz, J. P., Arbelo, M., Expósito, F. J., Podestá, G., Prospero, J. M., & Evans, R. (2001). Relationship between errors in AVHRR-derived sea surface temperature and the TOMS Aerosol Index. Geophysical Research Letters, 28, 1989-1992. https://doi.org/10.1029/2000GL012446

Gelaro, R., et al. (2017). The Modern-Era Retrospective Analysis for Research and Applications, Version 2 (MERRA-2). Journal of Climate, 30, 5419–5454. https://doi.org/10.1175/JCLI-D-16-0758.1

Good, E. J., Kong, X., Embury, O., & Merchant, C. J. (2012). An infrared desert dust index for the along-track scanning radiometers, Remote Sensing of Environment, 116, 159–176, https://doi.org/10.1016/j.rse.2010.06.016

Griggs, M. (1985), A method to correct satellite measurements of sea surface temperature for the effects of atmospheric aerosols, Journal of Geophysical Research**,** 90(D7), 12951–12959. https://doi.org/10.1029/JD090iD07p12951

Hess, M., Koepke, P., & Schult, I. (1998). Optical properties of aerosols and clouds: The software package OPAC. Bulletin of the American Meteorological Society, 79, 831–844. https://doi.org/10.1175/1520-0477(1998)079<0831:OPOAAC>2.0.CO;2

Ignatov, A., Zhou, X., Petrenko, B., Liang, X., Kihai, Y., Dash, P., Stroup, J., Sapper, J., & DiGiacomo, P. (2016). AVHRR GAC SST Reanalysis version 1 (RAN1). Remote Sensing, 8(4), 315. https://doi.org/10.3390/rs8040315

Le Borgne, P., Péré, S., & Roquet, H. (2013). Night time detection of Saharan dust using infrared window channels: Application to NPP/VIIRS. Remote Sensing Environment, 137, 264–273. https://doi.org/10.1016/j.rse.2013.06.001

Liang, X.-M., Ignatov, A., & Kihai, Y. (2009), Implementation of the Community Radiative Transfer Model in Advanced Clear-Sky Processor for Oceans and validation against nighttime AVHRR radiances, Journal of Geophysical Research, 114, D06112. https://doi.org/10.1029/2008JD010960

Liang, X.-M., & Ignatov, A. (2011). Monitoring of IR clear-sky radiances over oceans for SST (MICROS). Journal of Atmospheric and Oceanic Technology, 28. https://doi.org/10.1175/JTECH-D-10-05023.1

Liang, X.-M., Sun, N., Ignatov, A., et al. (2017). Monitoring of VIIRS Ocean Clear-Sky brightness Temperatures against CRTM Simulations in ICVS for TEB/M Bands, Proceedings of SPIE, Vol. 10402, 104021S. https://doi.org/10.1117/12.2273443

May, D. A., Stowe, L. L., Hawkins, J. D., & McClain, E. P. (1992). A correction for Saharan dust effects on satellite sea surface temperature measurements, Journal of Geophysical Research, 97(C3), 3611–3619. https://doi.org/10.1029/91JC02987

Merchant, C. J., Embury, O., Le Borgne, P., & Bellec, B. (2006). Saharan dust in night-time thermal imagery: Detection and reduction of related biases in retrieved sea surface temperature, Remote Sensing of Environment, 104, 15–30. https://doi.org/10.1016/j.rse.2006.03.007

Merchant, C. J., Harris, A. R., Murray, M. J., & Závody, A. M. (1999). Toward the elimination of bias in satellite retrievals of sea surface temperature: 1. Theory, modeling and interalgorithm comparison, Journal of Geophysical Research, 104(C10), 23565–23578, https://doi.org/10.1029/1999JC900105

Merchant, C. J., Harris, A. R., Roquet, H., & Le Borgne, P. (2009). Retrieval characteristics of non-linear SST from AVHRR, Geophysical Research Letters, 36(L17604), https://doi.org/10.1029/2009GL039843.

McMillin, L. M. (1975). Estimation of sea surface temperatures from two infrared window measurements with different absorption. Journal of Geophysical Research, 80(36), 5113–5117. https://doi.org/10.1029/JC080i036p05113

McMillin, L. M., & Crosby, D. S. (1984). Theory and validation of the multiple window sea surface temperature technique. Journal of Geophysical Research, 89(C3), 3655–3661. https://doi.org/10.1029/JC089iC03p03655

Nalli, N. R., & Stowe, L. L. (2002). Aerosol correction for remotely sensed sea surface temperatures from the National Oceanic and Atmospheric Administration advanced very high resolution radiometer. Journal of Geophysical Research, 107(C10), 3172. https://doi.org/10.1029/2001JC001162

Petrenko, B., Ignatov, A., Kihai, Y., & Dash, P. (2016). Sensor-Specific Error Statistics for SST in the Advanced Clear-Sky Processor for Oceans. Journal of Atmospheric and Oceanic Technology, 33, 345-359. https://doi.org/10.1175/JTECH-D-15-0166.1

Petrenko, B., Ignatov, A., Kihai, Y., Stroup, J., & Dash, P. (2014). Evaluation and selection of SST regression algorithms for JPSS VIIRS. Journal of Geophysical Research, 119(8), 4580-4999, https://doi.org/ doi:10.1002/2013JD020637

Pierangelo, C., Chédin, A., Heilliette, S., Jacquinet-Husson, N., & Armante, R. (2004). Dust altitude and infrared optical depth from AIRS, Atmospheric Chemistry and Physics, 4, 1813-1822, https://doi.org/10.5194/acp-4-1813-2004

Prabhakara, C., Dalu, G., & Kunde, V. G. (1974). Estimation of sea surface temperature from remote sensing in the 11- to 13-μm window region. Journal of Geophysical Research, 79(33), 5039–5044. https://doi.org/10.1029/JC079i033p05039

Reynolds, R. W. (1993). Impact of Mount Pinatubo aerosols on satellite-derived sea surface temperatures. Journal of Climate, **6**, 768–774. https://doi.org/10.1175/1520-0442(1993)006<0768:IOMPAO>2.0.CO;2

Saha, K., Ignatov, A., Liang, X.-M., & Dash, P. (2012). Selecting a first-guess sea surface temperature field as input to forward radiative transfer models. Journal of Geophysical Research, 117, C12001. https://doi.org/10.1029/2012JC008384

Saunders, R.W., Matricardi, M., & Brunel, P. (1999). An Improved Fast Radiative Transfer Model for Assimilation of Satellite Radiance Observations. Quarterly Journal of the Royal Meteorological Society, 125, 1407-1425. https://doi.org/10.1002/qj.1999.49712555615

Xi, X., & Sokolik, I. N. (2012). Impact of Asian dust aerosol and surface albedo on photosynthetically active radiation and surface radiative balance in dryland ecosystems. Advances in Meteorology, vol. 2012, Article ID 276207. https://doi.org/10.1155/2012/276207

Xi, X., & Sokolik, I. N. (2015). Dust interannual variability and trend in Central Asia from 2000 to 2014 and their climatic linkages. Journal of Geophysical Research, 120, 12,175–12,197. https://doi.org/10.1002/2015JD024092

Xi, X., & Sokolik, I. N. (2016). Quantifying the anthropogenic dust emission from agricultural land use and desiccation of the Aral Sea in Central Asia. Journal of Geophysical Research, 121, 12,270-12,281. https://doi.org/10.1002/2016JD025556

Yang, P., et al. (2007), Modeling of the scattering and radiative properties of nonspherical dust-like aerosols, Journal of Aerosol Science, 38(10), 995–1014. https://doi.org/10.1016/j.jaerosci.2007.07.001

Table 1. Global statistics of the nighttime O-M BT biases in SNPP VIIRS SST bands M12 and M14-16, based on aerosol-free simulations for 18-31 January 2018.

| | M12/3.7 μm | | M14/8.6 μm | | M15/11 μm | | M16/12 μm | |
|---|---|---|---|---|---|---|---|---|
| | Median | RSD | Median | RSD | Median | RSD | Median | RSD |
| CRTM+GFS | -0.145 | 0.308 | -0.714 | 0.458 | -0.575 | 0.485 | -0.728 | 0.583 |
| CRTM+MERRA2 | -0.114 | 0.305 | -0.626 | 0.441 | -0.464 | 0.464 | -0.599 | 0.551 |
| RTTOV+MERRA2 | +0.003 | 0.370 | -0.391 | 0.589 | -0.087 | 0.626 | -0.096 | 0.779 |

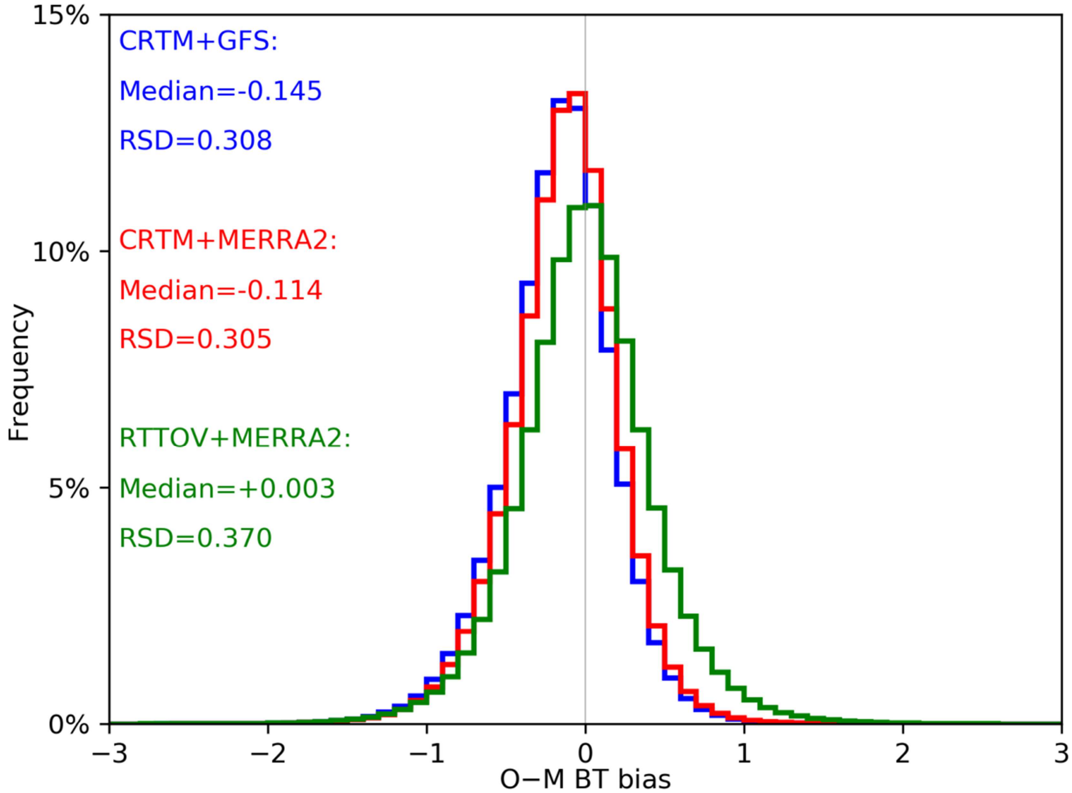


Figure 1. Global histograms of nighttime O-M BT biases in the SNPP VIIRS band M12 (3.7 µm) based on three experiments for the study period of 18-31 January 2018. The corresponding median biases and RSDs for all four SST bands (M12, and M14-16) are summarized in Table 1.

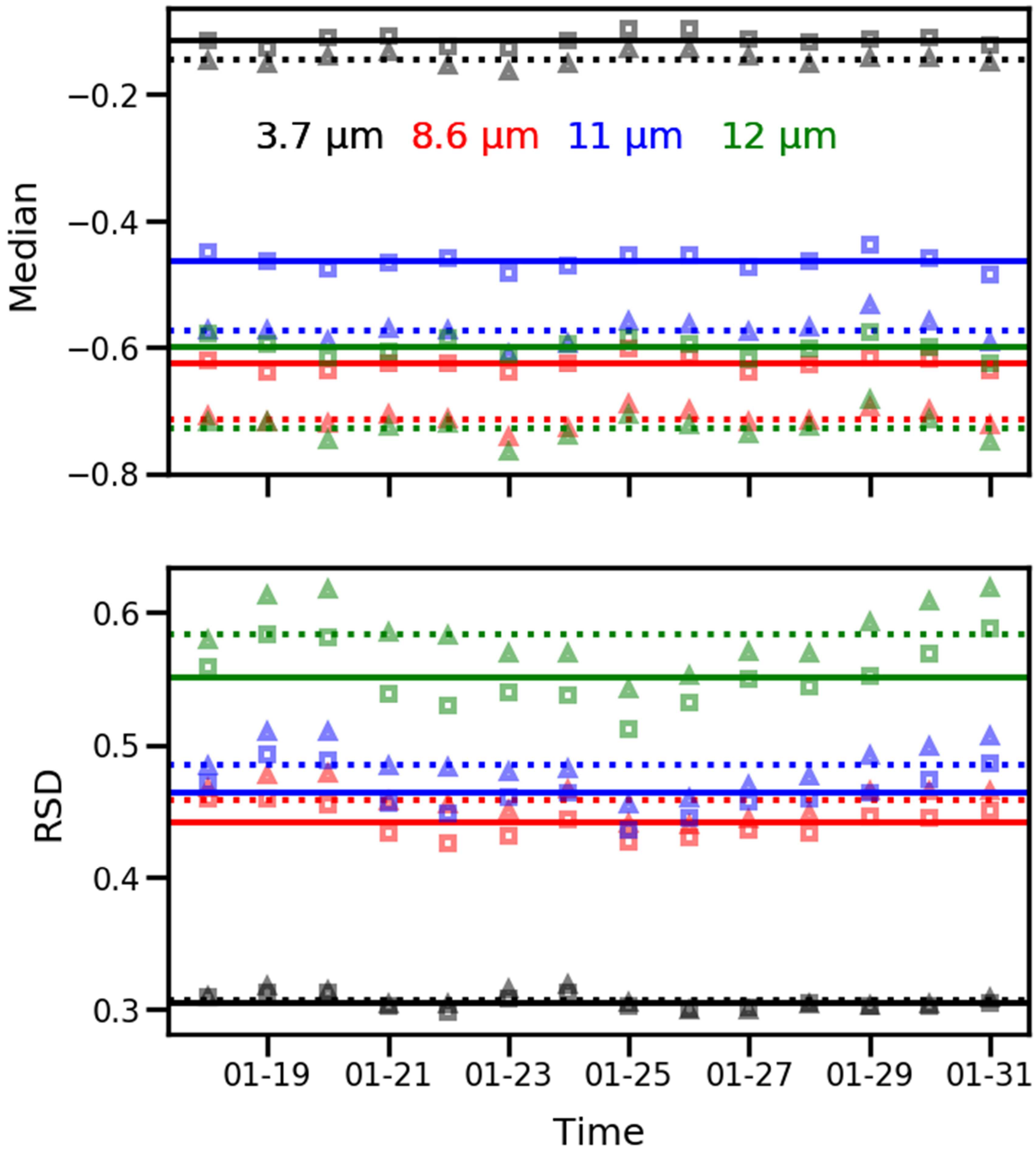


Figure 2. Time series of the global nighttime O-M BT median biases (top) and RSDs (bottom) in the four SNPP VIIRS IR SST bands based on ACSPO CRTM simulations using GFS (triangles; broken lines) and MERRA-2 (squares; solid lines) profiles. Each symbol represents daily global statistics and the horizontal lines represent averages over the study period.

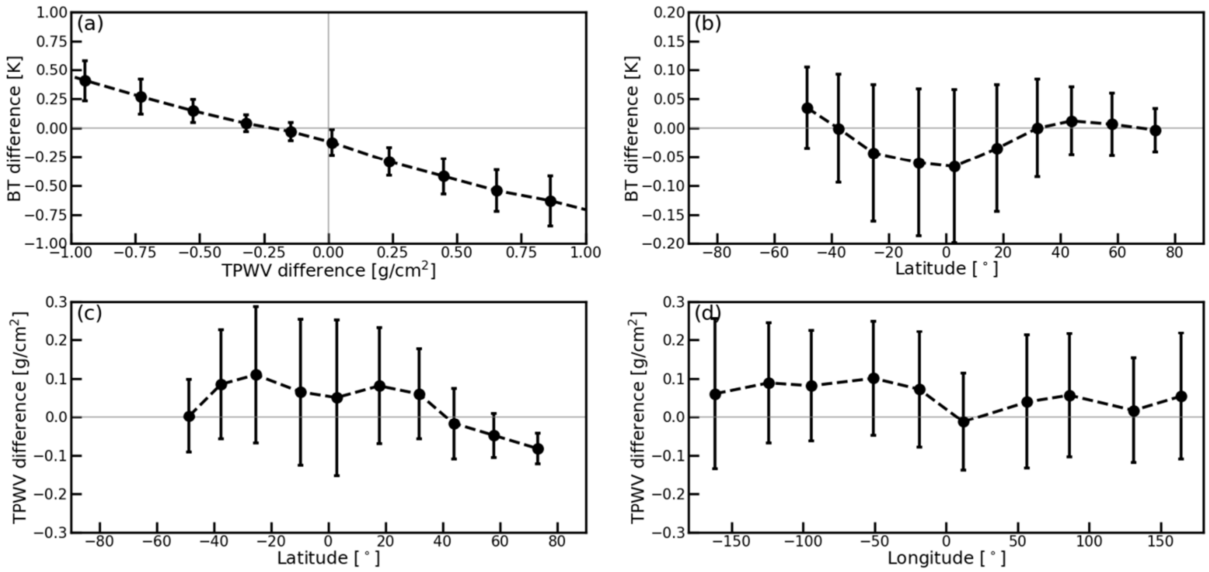


Figure 3. ACSPO/CRTM simulated BT difference in the SNPP VIIRS band M12 (3.7 μm) using MERRA-2 versus GFS meteorological profiles, as a function of the difference in column total precipitable water vapor (TPWV) between MERRA-2 and GFS (a); Same as (a), but as a function of latitude (b); The TPWV difference between MERRA-2 and GFS as a function of latitude (c) and longitude (d). All results are derived from the study period of 18-31 January 2018.

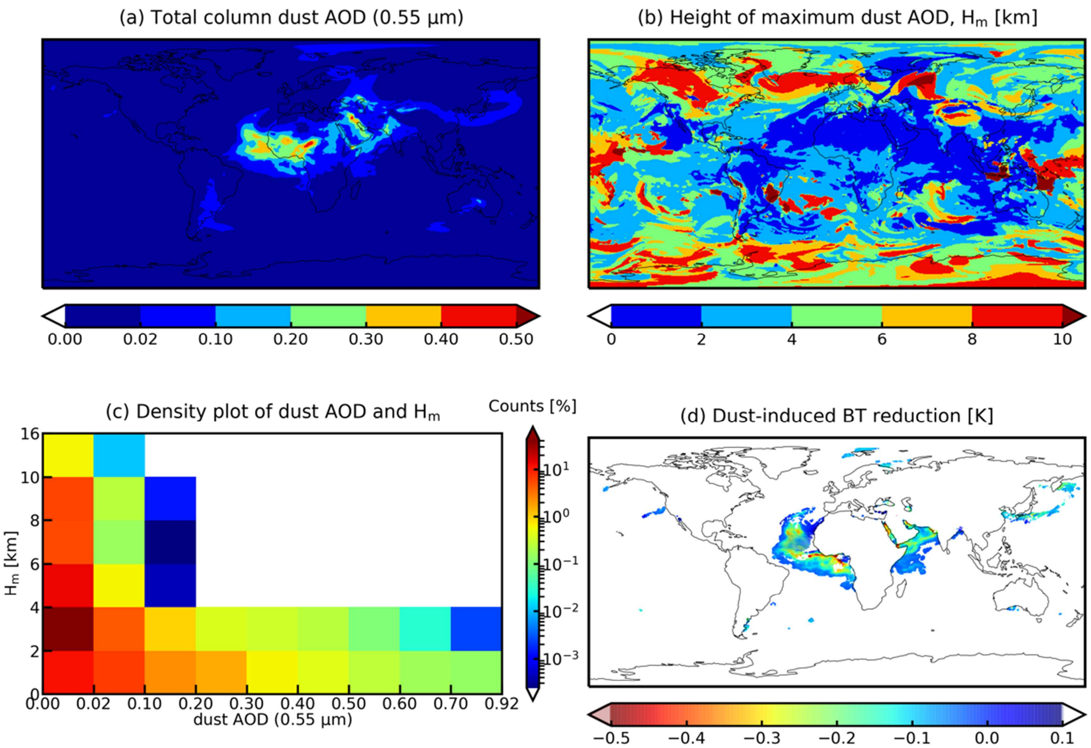


Figure 4. MERRA-2 total column dust AOD at 0.55 μm on 23 January 2018 (a); Vertical height ($H_m$) associated with the maximum dust AOD (b); Density plot of dust AOD and $H_m$ (c); RTTOV simulated increments in the nighttime BT due to dust in the 3.7 μm band (d).

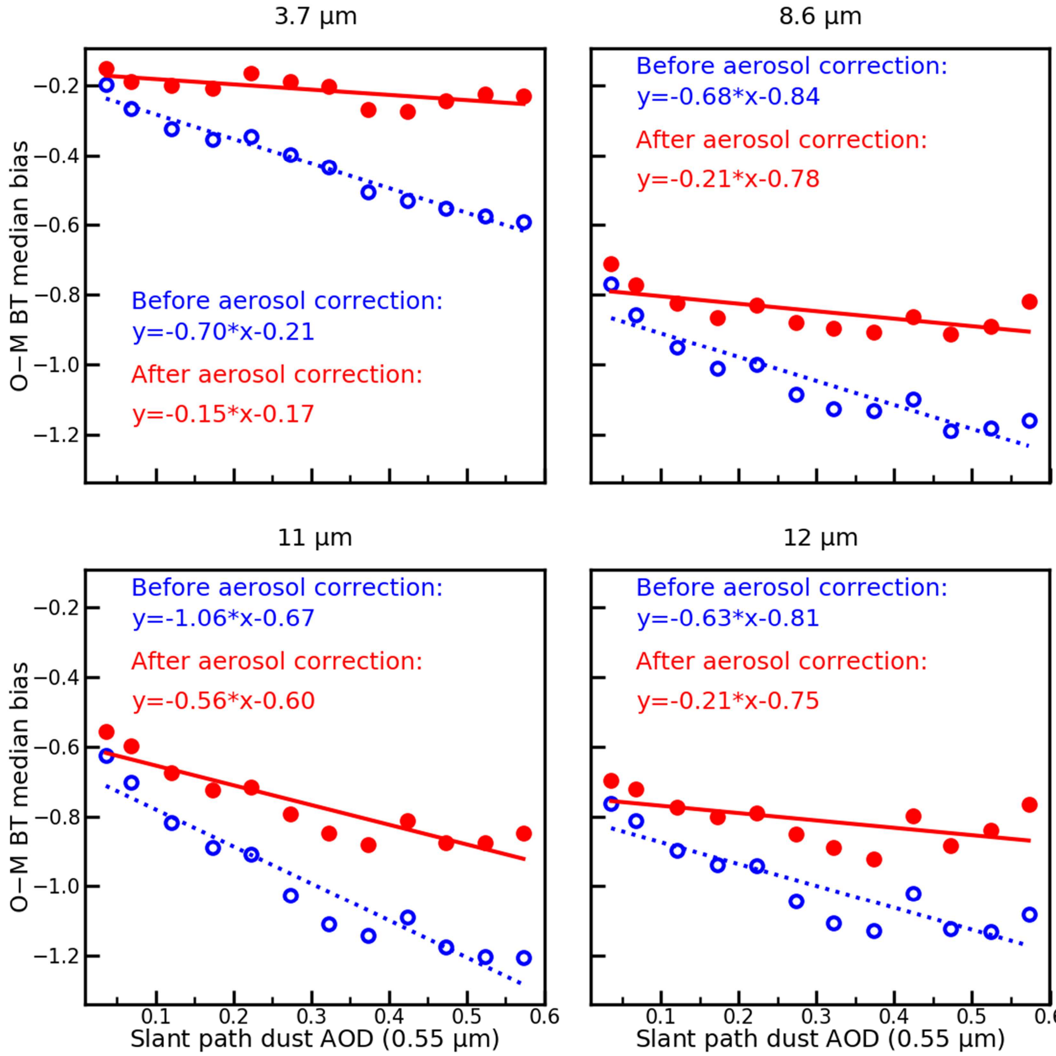


Figure 5. ACSPO O–M BT biases as a function of dust AOD for global nighttime SNPP VIIRS data from 18-31 January 2018, based on CRTM simulations using MERRA-2 profiles, without (blue) and with (red) dust aerosol correction.

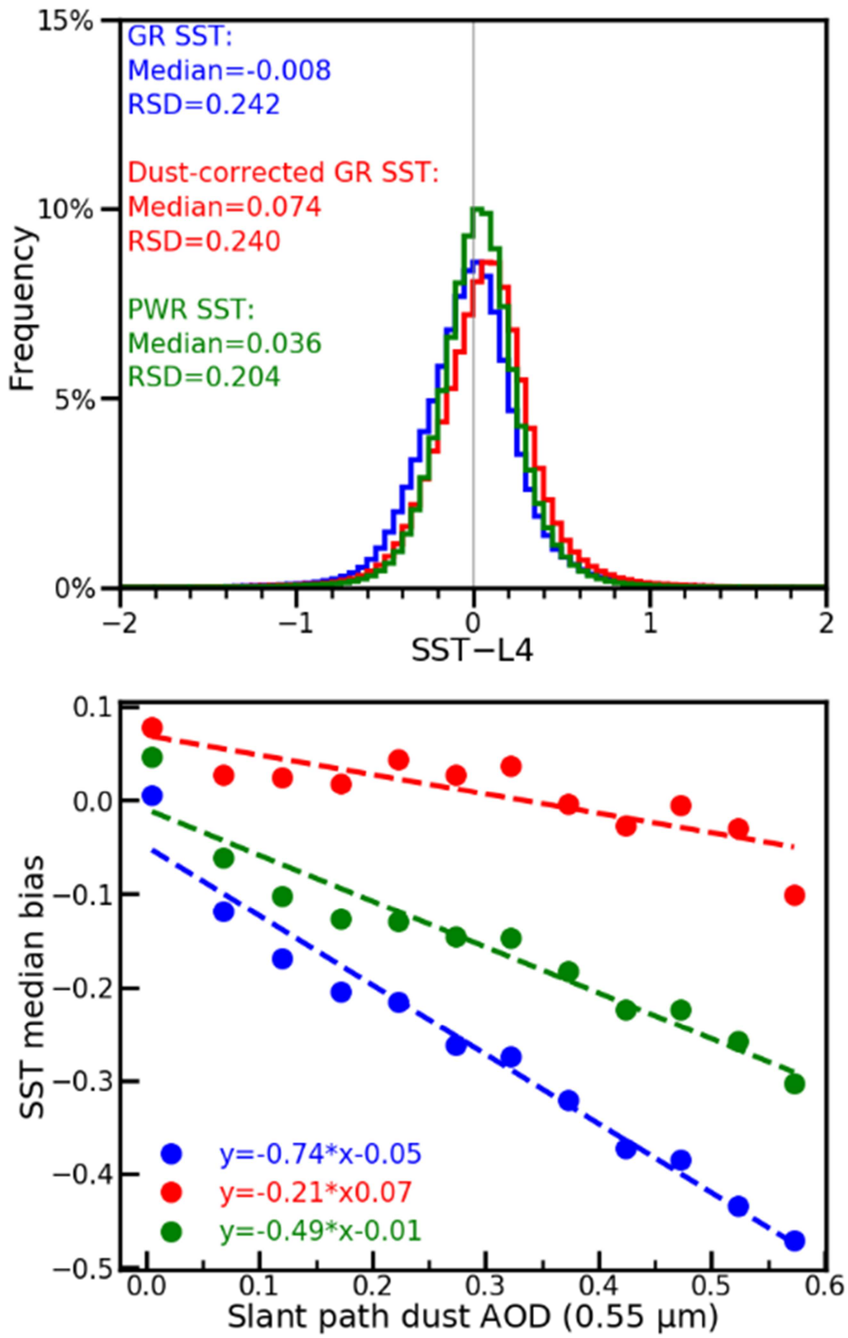


Figure 6. Global histograms of ACSPO SST biases with respect to the CMC L4 (top); Changes in the SST median biases as a function of dust AOD (bottom). Three SST products are considered: ACSPO global regression SST (GR SST), GR SST derived from aerosol-corrected

VIIRS BTs, and ACSPO piecewise regression SST (PWR SST), all based on global nighttime data of SNPP VIIRS from 18-31 January 2018.

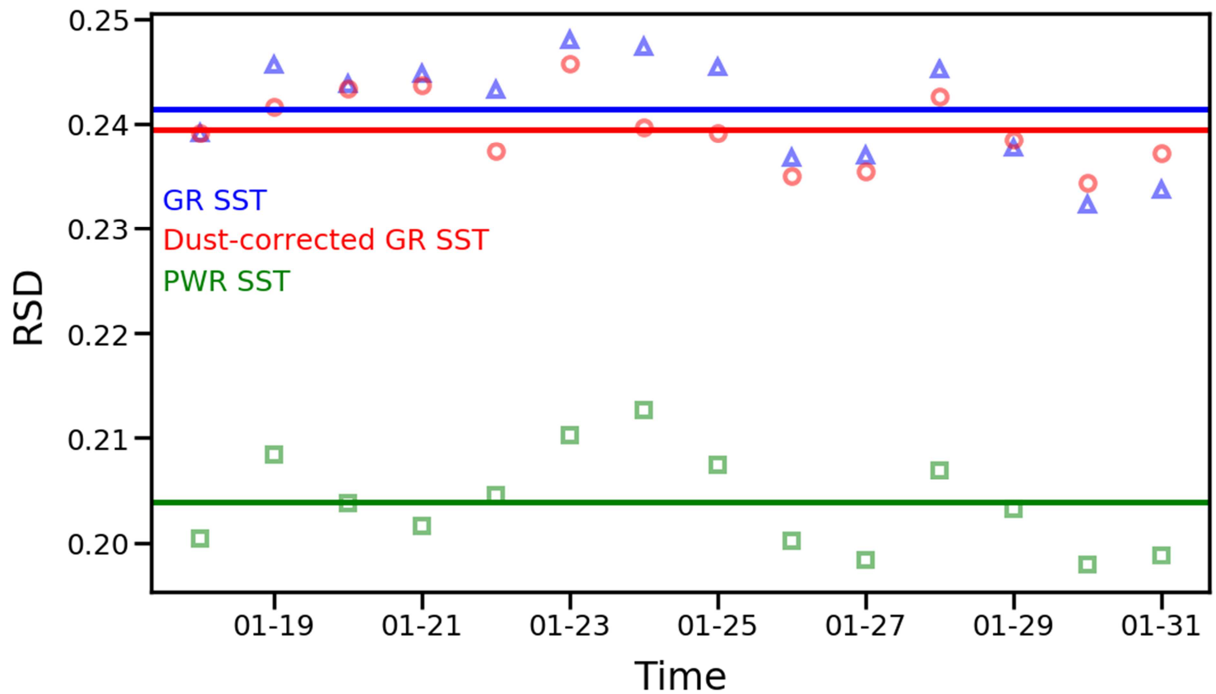


Figure 7. Time series of the RSDs of three SST products shown in Figure 6.